Journal of Marine Science and Application (2025) 24: 959-969
https://doi.org/10.1007/s11804-025-00641-4

RESEARCH ARTICLE

Experimental Study on Vortex-Induced Vibration of Underwater Manipulator Under Shear Flow

Senliang Dai[1], Derong Duan[1], Xin Liu[2], Huifang Jin[1], Hui Zhang[1] and Xuefeng Yang[1]

Received: 04 July 2024 / Accepted: 28 August 2024

Abstract
The position deviation of the underwater manipulator generated by vortex-induced vibration (VIV) in the shear flow increases relative to that in the uniform flow. Thus, this study established an experimental platform to investigate the vibration characteristics of the underwater manipulator under shear flow. The vibration response along the manipulator was obtained and compared with that in the uniform flow. Results indicated that the velocity, test height, and flow field were the main factors affecting the VIV of the underwater manipulator. With the increase in the reduced velocity (U_r), the dimensionless amplitudes increased rapidly in the in-line (IL) direction with a maximum of 0.13D. The vibration responses in the cross-flow (CF) and IL directions were concentrated at positions 2, 3 and positions 1, 2, with peak values of 0.46 and 0.54 mm under U_r = 1.54, respectively. In addition, the vibration frequency increased with the reduction of velocity. The dimensionless dominant frequency in the CF and IL directions varied from 0.39 – 0.80 and 0.35 – 0.64, respectively. Moreover, the ratio of the CF and IL directions was close to 1 at a lower U_r. The standard deviation of displacement initially increased and then decreased as the height of the test location increased. The single peak value of the standard deviation showed that VIV presented a single mode. Compared with the uniform flow, the maximum and average values of VIV displacement increased by 104% and 110% under the shear flow, respectively.

Keywords Underwater manipulator; Shear flow; Vortex-induced vibration; Spectral analysis; Vibration response

1 Introduction

With the rapid increase in the demand for marine resources, underwater manipulators have played a crucial role in underwater operations in recent years (Carlucho et al., 2021; Duan et al., 2023). As a typical cylindrical structure, alternating vortexes are produced when manipulators are subjected to fluid flow. The results indicate that the underwater manipulator generates vortex-induced vibration (VIV) due to the presence of alternating vortices (Mao et al., 2023), thereby reducing the positioning accuracy and structural stability. Thus far, many researchers have conducted the VIV experiment to study the vibration characteristics of marine equipment (Kang et al., 2016; Wang et al., 2022).

Numerous scholars have modeled the manipulator as a cylindrical link (Kolodziejczyk, 2018). However, the flow characteristics of the underwater manipulator were more complex than the flow around an infinite cylinder. In addition, the underwater motion of the manipulator experiences interferences among its multiple arms. McLain and Rock (1998) tested the hydrodynamic force of the single-degree-of-freedom underwater manipulator, revealing that the hydrodynamic coefficient of the manipulator changed with motion. Kolodziejczyk (2016; 2023) explored the hydrodynamic loads of underwater manipulators in different postures. Meanwhile, the time history of hydrodynamic loads with the periodic change in fluid speed was discussed. Cheng et al. (2022) conducted the effect of cross-section shape on the hydrodynamic coefficient and flow field of the underwater manipulator by numerical calculation, demonstrating that the manipulator was more stable when arm 2 was located upstream. The early experimental research focused on the rigid cylinder, generally exploring the vertical direction of incoming flow. Mercier (1973) compared the vibration in the cross-flow (CF) and in-line (IL) directions and analyzed the relationship between dimensionless frequency

Article Highlights

- The vortex-induced vibration displacement reaches the highest at 0.13D.
- When U_r = 1.54, the peak values in CF and IL directions are 0.46 and 0.54 mm.
- The dimensionless frequency in the two directions is less than 1.
- Compared with uniform flow, the maximum displacement under shear flow increases by 104%.

✉ Derong Duan
me_duandr@ujn.edu.cn

[1] School of Mechanical Engineering, University of Jinan, Jinan 250022, China

[2] Zibo Non-public Sector Development Center, Zibo 255000, China

and amplitude of the cylinder at Reynolds number 600–13 000. Sarpkaya (1977) tested the vibration of a rigid cylinder with a diameter of 19–38 mm in the CF direction at Reynolds number from 500 to 25 000. They established the relationship of drag force, lift force, and other force coefficients with the reduction velocity and dimensionless frequency. Gopalkrishna (1993) discussed the forced vibration in the CF direction of an aluminum cylinder with a length–diameter ratio of 24, revealing the law of lift coefficient that varies with dimensionless amplitude and frequency. Bahmani and Akbari (2010) conducted the dynamic response of an elastically mounted cylinder in laminar flow. When the Reynolds number was between 80 and 160, the vibration amplitude was enhanced due to the decrease in the mass ratio and damping ratio in the system.

With the development of ocean engineering, the research object gradually changed to the flexible riser with a high aspect ratio in the uniform flow field. Griffin and Vandiver (1984) investigated the acceleration signals of a steel pipe with a length-diameter ratio of 558 and a cable with a length-diameter ratio of 715 in an actual underwater environment. This finding reveals that the vibration frequency of the cable was evidently affected by the sag. In a towed tank, de Wilde and Huijsmans (2004) used a grating fiber sensor to test the VIV response of 12.6 m steel pipe in the CF and IL directions. The results demonstrated a strong coupling between CF and IL directions and a phenomenon of multimode response. Allen and Henning (2001) analyzed the vibration displacement and dominant mode of a cylinder with a diameter of 0.06 m, indicating that the cylinder displacement at each end was close to high Reynolds numbers. Tongarelli et al. (2004) considered the riser surface strain and displacement using strain gauges and uniaxial acceleration sensors. They noted that the response frequency increased with the increase in flow speed. Gao et al. (2016) examined the VIV response of a flexible cylinder in the CF and IL directions under uniform flow using the mode superposition method. They found the relationship between the reduction velocity and displacement. When the reduction velocity was low, the response frequency participated in the entire VIV. Mao et al. (2015) explored the VIV feature parameters, such as the displacement and dominant frequency of the sediment pipe, demonstrating that the response frequency of the water pipe in the same direction was consistent. Kumar and Nallayarasu (2022) obtained the root mean square of CF direction displacement in the flexible riser along the pipe under different shear flow conditions. The results indicated that the displacement increased as the slope decreased. Zhu et al. (2021) assessed the effect of vortex excitement and solid structure on the acceleration, displacement, and dominant modulus of a cylinder, showing that the response of amplitude and frequency increased with the increase in speed. Zhang et al. (2020) studied the vibration amplitude and frequency characteristics of a large length-diameter ratio cylinder under the coupled flow field at Reynolds number from 2 000 to 24 000. They found that the CF amplitude increased with the increase in oscillation amplitude or frequency at low and medium reduction velocities. Seyed-Aghazadeh et al. (2021) leveraged a wind tunnel test of a large-quality cylinder to study the vibration characteristics of a single and series cylinder. They found that the amplitude increased with the increase in the spacing of the two cylinders.

In these studies, VIV is a common phenomenon in marine engineering, inducing fatigue damage to marine structures. At present, researchers mainly investigate the VIV of cylindrical structures under uniform flow, such as risers, catenaries, and pipes. However, the VIV phenomenon also occurs during the operation of the underwater manipulator with a large aspect ratio, affecting the precise control of the manipulator. Moreover, the variable posture of the working manipulator produces shear flow, resulting in more complex VIV responses (Xue et al., 2019). Therefore, to clarify the vibration characteristics of the underwater manipulator, its VIV under shear flow was investigated. The vibration response of the manipulator along the arm position was analyzed by building a VIV test bench under shear flow and compared with the VIV response under uniform flow.

The structure of this work is as follows: Initially, the acceleration signal is tested by an independently designed VIV experimental platform of the underwater manipulator. Then, the effects of various parameters on the VIV of the underwater manipulator are discussed. Finally, the conclusions are summarized.

2 Experimental set-up

2.1 Description of experimental platform

As depicted in Figure 1, the test was performed in a self-designed VIV experimental platform of an underwater manipulator. Figure 1(a) shows the schematic diagram of the shear flow structure. The instantaneous flow state between the manipulator and the still water was realized by rotating motion to overcome the limitations of the site and motion path in the towing tank test, according to the principle of relative motion. Figure 1(b) illustrates the composition of the test device, including the power supply, motor, data acquisition, underwater manipulator, acceleration sensor, slide ring, pool, computer, and rotation rod. The computer controlled the rotation of the rod, to which the underwater manipulator was fixed. To solve the problem of line entanglement during rotational motion, an electronic slip ring was installed between the motor and the rotating rod, enabling the acquisition and transmission of acceleration signals. The tilted posture of the manipulator can generate a stable linear shear flow field (Fu et al., 2022). When the manipu-

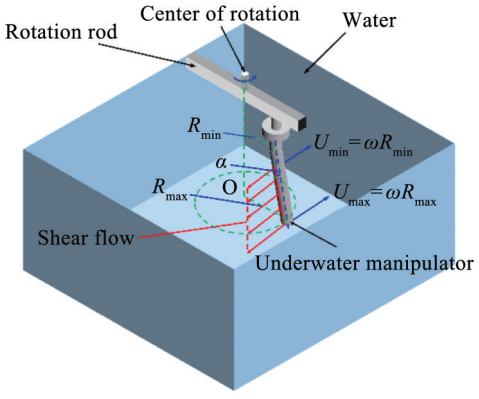

(a) Schematic diagram of Shear flow

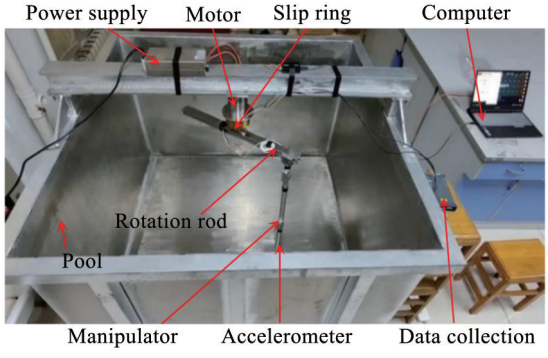

(b) Test flow voryex-induced vibration platform

Figure 1 Shear flow vortex-induced vibration platform

lator moves around the rotation center, its velocity at different positions in the tilt posture varies. The relationship between the velocity of the motor and the manipulator is expressed as follows:

$$U = \omega R = 2\pi n R \tag{1}$$

where U indicates the flow velocity of a point on the manipulator, R represents the distance between the manipulator and the rotation center, and n denotes the motor speed.

Therefore, the linear shear flow is expressed as follows:

$$U(y) = U_{min} + y\frac{U_{max} - U_{min}}{L} \tag{2}$$

where $U(y)$ represents the flow velocity at a certain position y of the underwater manipulator. U_{min} refers to the minimum velocity at the top. U_{max} denotes the maximum velocity at the bottom. L indicates the length of the underwater manipulator.

The parameters of the underwater manipulator model are shown in Table 1. The outer diameter D and inner diameter d of the manipulator were 30 and 15 mm, respectively. The length of the upper arm L_1 was 400 mm, and that of the lower arm L_2 was 300 mm. The upper and lower arms were connected by a revolute pair with a length of 50 mm.

Figure 2 displays the schematic diagram of the test position. Four positions, position 1, position 2, position 3, and position 4, were selected, considering the manipulator's end. The distances from these positions to the end of the manipulator were 20, 155, 370 and 550 mm. The tilted manipulator rotation around the center of rotation can produce a linear shear velocity. The SENTHER acceleration sensor was selected to test the vibration signals of the four positions. The direction of the horizontal flow was defined as the in-line (IL) direction, and the vertical flow direction was the cross-flow (CF) direction.

Table 1 Model parameter of the manipulator

Model parameter	Value
L_1 (m)	0.4
L_2 (m)	0.3
Joint (m)	0.05
Outer diameter (m)	0.03
Inner diameter (m)	0.015
Young's modulus (GPa)	72
Density (kg/m^3)	2.72×10^3
Poisson's ratio	0.34

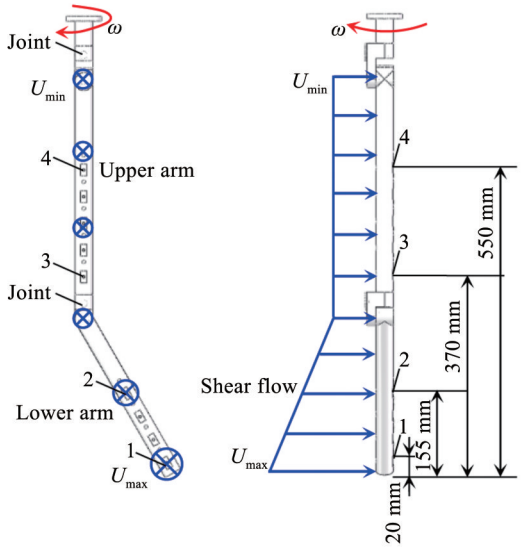

(a) Main view (b) Left view

Figure 2 Schematic of testing position

2.2 Experimental parameters

The test parameters were designed to be dimensionless to eliminate the influence of units and scale in the problem. The dimensionless amplitude A^* represents the ratio of the maximum displacement to a reference value. The formula is expressed as follows:

$$A^* = \frac{A}{D} \tag{3}$$

where A represents the amplitude of the manipulator structure.

The dimensionless dominant frequency f^* refers to the dimensionless vibration frequency. It is the ratio of the vibration frequency to the natural frequency, the formula of which is expressed as follows:

$$f^* = \frac{f}{f_n} \tag{4}$$

where f denotes the vibration frequency of the manipulator, and f_n indicates the natural frequency of the manipulator.

The Strouhal number S_t denotes the relationship between the instability of the boundary layer separation and the relatively stable vortex shedding frequency. The formula is expressed as follows:

$$S_t = \frac{f_s U}{D} \tag{5}$$

where f_s refers to the Strouhal frequency of the underwater manipulator.

2.3 Natural frequency analysis

The underwater manipulator was usually submerged in water, greatly affecting the modal characteristics of the underwater manipulator. Therefore, the wet modal characteristics of the underwater manipulator instead of its modal characteristics in the air must be explored to avoid frequency lock-in and resonance (Zhu et al., 2022). ANSYS software was widely used as a practical and fast simulation method in wet mode analysis. The 3D model was built by a Workbench design molder, including water, underwater manipulator and air. The relevant parameter settings are shown in Table 2. The underwater manipulator was defined as the fluid-solid coupling surface with a fixed constraint applied at its top. As a result, Table 3 presents the first six natural frequencies of the underwater manipulator in still water.

Table 2 Modal analysis parameter settings

Material	Aluminum Alloy	Air	Water
Minimum yield strength (MPa)	231	-	-
Tensile strength (MPa)	265	-	-
Density (kg/m^3)	2 650	1.29	1 000
Elastic Modulus (MPa)	72 000	-	2 180
Poisson's ratio	0.3	-	0.5
Sound speed (m/s)	-	340	1 500

2.4 Test condition

Figure 1(a) illustrates that the flow velocity of the test condition was changed by adjusting the motor speed. In view of the universality of the research, in the present experiment, the reduction velocity (U_r) was used to investigate the vibration characteristics of the underwater manipulator. The calculation formula is as follows:

Table 3 Natural frequency of the underwater manipulator

Order-number	Frequency (Hz)
1	28.208
2	33.973
3	158.67
4	189.53
5	473.87
6	544.68

$$Re = \frac{\rho U D}{\mu} \tag{6}$$

$$U_r = \frac{U}{f_n D} \tag{7}$$

where Re, ρ, and μ represent Reynolds number, fluid density, and dynamic viscosity coefficient, respectively. U denotes the flow velocity, $U = U_{\min}$. The diameter of the cylinder $D = 0.03$ m, f_n indicates the natural frequency of the underwater manipulator.

Table 4 suggests that the reduction velocity was low. The control mode of the VIV of the underwater manipulator is maintained at stage one. Therefore, the flow velocity in the test was outside the flow velocity range when the frequency lock-in occurred (Aswathy and Sarkar, 2019).

Table 4 Test conditions for the vortex-induced vibration

Work conditions	Re	Flow velocity (m/s)	Reduction velocity
1	12 000	0.40	0.54
2	16 000	0.53	0.72
3	20 000	0.67	0.90
4	30 000	1.00	1.18
5	34 000	1.13	1.36
6	38 000	1.27	1.54

2.5 Test data processing method

The method of frequency domain integration was employed to explore the law of VIV response (Liu et al., 2020). The related formulas are as follows.

The formula for the first integration calculation is as follows:

$$y(r) = \sum_{N-1}^{k=0} \frac{1}{\mathrm{j}2\pi k \Delta f} H(k) X(k) \mathrm{e}^{\mathrm{j}2\pi k r/N} \tag{8}$$

The formula for the second integration calculation is as follows:

$$y(r)=\sum_{N-1}^{k=0}\frac{-1}{(2\pi k\Delta f)^2}H(k)X(k)\,\mathrm{e}^{\mathrm{j}2\pi kr/N} \tag{9}$$

$$H(k)=\begin{cases}1 & (f_d\leqslant kf\leqslant f_u)\\ 0 & (\text{else})\end{cases} \tag{10}$$

f_d and f_u in the formula represent the lower limit frequency and the upper limit of the deadline. $X(k)$ denotes the Fourier transformation of $x(r)$, and f refers to the frequency resolution. The above formula indicates that the acceleration signal can be converted into displacement, facilitating the next-step data processing.

2.6 Error analysis

The test error in the experiment leads to randomness and uncertainty of the test results (Wu et al., 2022). The reliability of the test results was verified through multiple measurements and the standard deviation calculation, representing the dispersion of the data. A smaller standard deviation indicates greater measurement accuracy. In the test, the random error was approximated by the standard deviation, as shown in the following equation:

$$S=\sqrt{\frac{\sum_{n}^{i=1}\left(x_i-\bar{x}\right)^2}{n-1}} \tag{11}$$

The vibration response of the underwater manipulator at U_r = 0.53 was measured several times. The displacement spectrum was obtained by quadratic integral and fast Fourier transform. Table 5 shows the dominant frequency (f) and displacement amplitude (A) of position 1 in the CF direction. In Table 5, the main frequency of vibration obtained from the multiple tests was approximately 11.70 Hz. The standard deviation between the tests was 0.006 mm, indicating that the test data were close to the average value and the measurement value was more accurate. The maximum relative error between displacement amplitude and displacement mean value obtained by multiple tests was 1.17%. In summary, the test results had excellent repeatability and reliability.

Table 5 Error analysis of the test system

Test	1	2	3	4
f (Hz)	11.72	11.69	11.70	11.71
A (mm)	0.50	0.49	0.50	0.49

3 Results and discussion

3.1 Vortex-induced vibration response of underwater manipulator

When the underwater manipulator was operated, the end of the underwater manipulator was more susceptible to environmental disturbances, requiring higher positioning accuracy. Figures 3 and 4 illustrate the displacement time history curve and spectrum diagram of position 1 in the CF and IL directions. In the figure, changing trends of the displacement time history curve in the CF and IL directions were relatively clear. The vibration displacement of position 1 increased with the reduction velocity. Moreover, the vibration displacement in the IL direction was significantly larger than that in the CF direction. At different reduction velocities, the dominant frequency in the CF and IL directions was evident, and high-frequency vibration was observed.

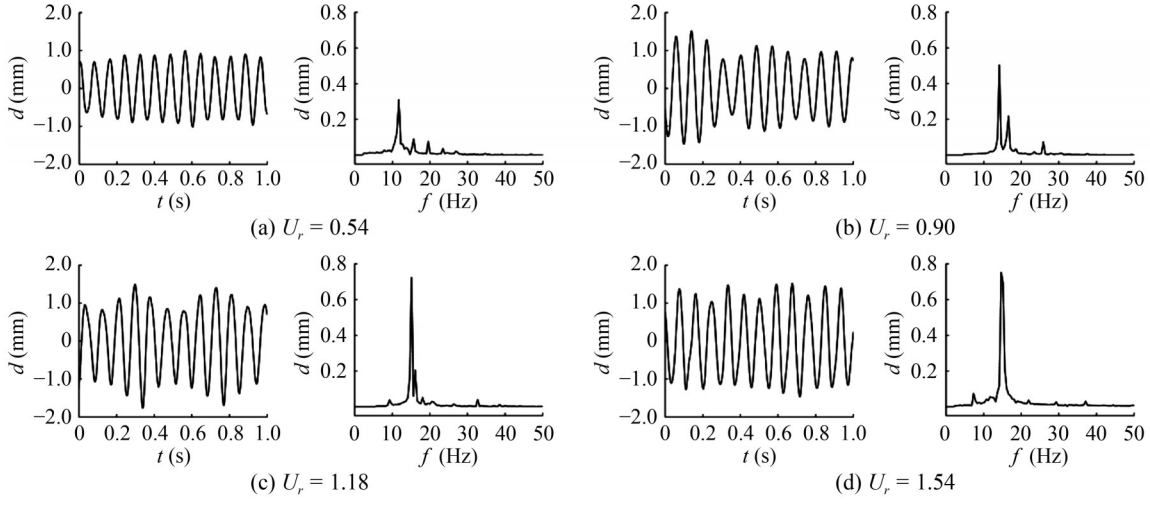

Figure 3 Time history curve and spectrum diagram of CF displacement

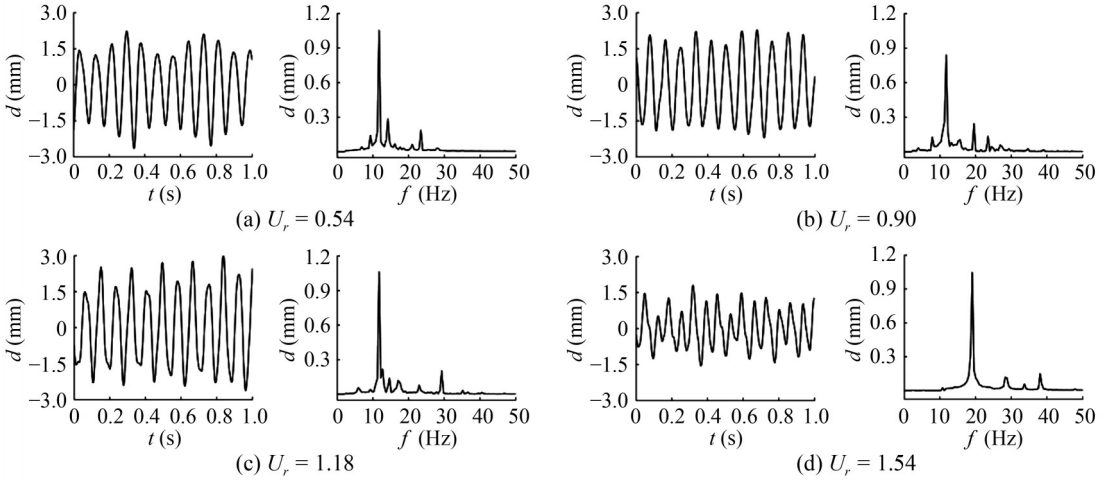

Figure 4 Time history curve and spectrum diagram of IL displacement

In Figure 3, when U_r = 0.54, the displacement time history curve in the CF direction was smooth, and the corresponding vibration frequency was 11.72 Hz. Under the conditions of 0.90, 1.18 and 1.54, the displacement amplitude increased as the reduction velocity increased. Naturally, a certain fluctuation was found in the displacement time history curve. The main frequency of vibration increased greatly in the spectrum diagram. With the excitation of high velocity, the vibration frequency in the CF direction of the underwater manipulator reached approximately 20 Hz, which was close to the natural frequency of the manipulator.

As depicted in Figure 4, the vibration displacement in the IL direction was larger than that in the CF direction. The spectrum diagram exhibited a high vibration frequency. The displacement response and main vibration frequency exhibited a pattern similar to that in the CF direction. The displacement in the IL direction was approximately twice that in the CF direction. As the reduction velocity increased, the gap between the displacements in the two directions decreased gradually. This phenomenon differed from traditional riser VIV experiments, where the riser, affected by vortex shedding, experienced VIV predominantly influenced by the lift force in the CF direction (Gao et al., 2020). Thus, the displacement in the IL direction was greater than that in the CF direction. However, owing to variations in materials, structural forms, and installation methods of the underwater manipulator, the drag force in the IL direction was more pronounced, leading to a rapid increase in displacement in that direction (Chen et al., 2015).

3.2 Dimensionless displacement of local position

Figure 5 demonstrates the variation of dimensionless amplitude in the CF and IL directions of the underwater manipulator. The figure evidently shows that the dimensionless amplitude in the CF and IL directions increased with velocity reduction. At the same time, some differences appeared in the amplitude at different test positions.

The dimensionless amplitude of positions 1 and 2 had a larger fluctuation. When U_r = 0.72, the dimensionless amplitudes of positions 1 and 2 were 0.067D and 0.043D, respectively. Subsequently, the amplitude of both positions began to decline. When U_r = 0.9, the speed of decline slowed down. Then, the trend of dimensionless amplitude continued to increase gradually. When U_r = 1.54, the amplitude at positions 1 and 2 reached 0.043D and 0.054D, respectively. In addition, similar variation rules were found at positions 3 and 4. Within the reduction velocity range of 0.54–0.72, the amplitude at positions 3 and 4 of the underwater manipulator decreased slightly. When U_r > 0.9, the trend at positions 3 and 4 began to rise steadily. Eventually, the maximum values of the dimensionless amplitude at U_r = 1.54 were 0.061D and 0.043D, respectively. The position near the end of the underwater manipulator was more prone to vibrate under the action of low flow velocity. In general, the dimensionless amplitude of the underwater manipulator increased gradually under the reduction velocity range of 0.54–1.54. In the study of cylindrical VIV, a rapid upward trend of amplitude under the low reduction velocity was found in the CF direction (Sun et al., 2023), consistent with the variation law of dimensionless amplitude in this work. Thus, as shown in Figure 5, the VIV at the end of the underwater manipulator must receive considerable attention.

The figure also shows some differences in the dimensionless amplitudes of the IL direction at different locations under the reduction velocity of 0.54–1.54. The average values of the four locations were all controlled below 0.04D. When U_r = 1.54, the dimensionless amplitude in the IL direction reached the peak with the increase in velocity reduction. The maximum values of amplitude at positions 1, 2, 3, and 4 were 0.10D, 0.09D, 0.12D, and 0.08D, respectively. Compared with the CF direction, the dimensionless amplitude in the IL direction increased by 150%, 80%, 200%, and 40%. The amplitude in the IL direction was

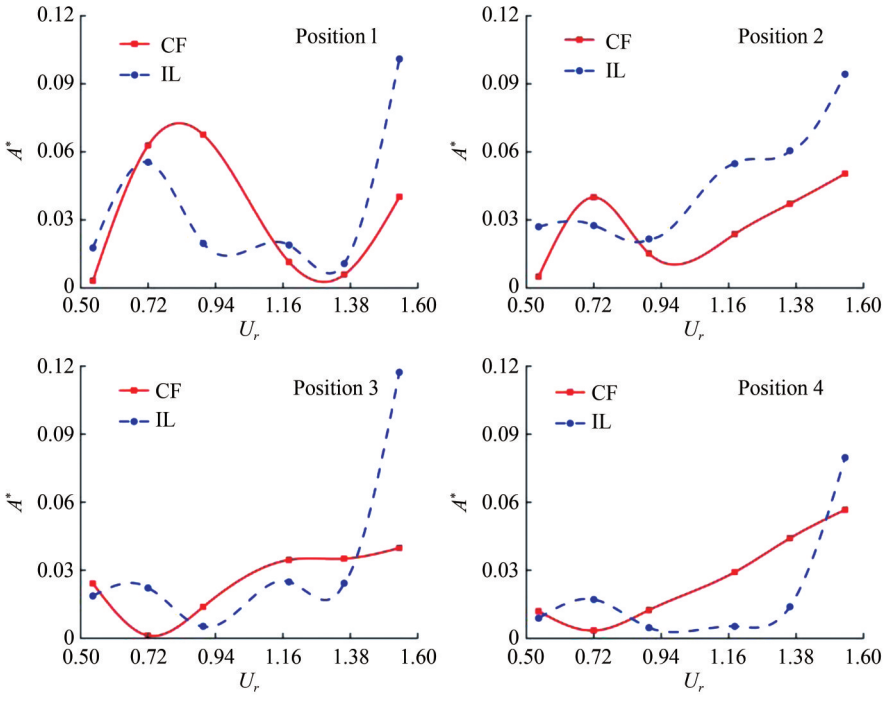

Figure 5 Variation of amplitude with reduction velocity at different positions in CF and IL directions

greater than that in the CF direction, as described in the previous content. It was mainly affected by the drag force in the IL direction. The dimensionless amplitude in the IL direction also increased with the reduction in velocity (Capell et al., 2019).

Figure 6 illustrates the spatial distribution of the displacement standard deviation in the CF and IL directions. Figure 6(a) shows that when U_r = 0.54, the peak of the standard deviation of the vortex-induced vibration displacement appeared near the test position 3. The standard deviation of displacement was small under this flow velocity condition. In the range of U_r = 0.72–1.54, with the increase in velocity reduction, the displacement standard deviation increased. When U_r = 1.54, the peak value in the CF direction was 0.46 mm. In summary, the standard deviation of the VIV displacement in the CF direction initially increased and then decreased with the increase in test height. In this process, the displacement peak in the CF direction was unique and presented a single mode. The vibration response was mainly concentrated in the middle section of the underwater manipulator. This phenomenon was similar to the research results in the VIV experiment of traditional risers (Liu et al., 2023).

As shown in Figure 6(b), the symmetry of displacement standard deviation in the IL direction was poor, and the amplitude remained below 0.6 mm. Compared with the CF direction, the displacement gap between velocity conditions was small, and the peak value of the displacement standard deviation appeared at position 2. Similarly, the standard deviation of VIV displacement in the IL direction increased initially and then decreased with the test height. A larger velocity resulted in larger displacement. In the IL direction, the displacement peak of the standard deviation was single, resulting in the maximum value of 0.54 mm under U_r = 1.54.

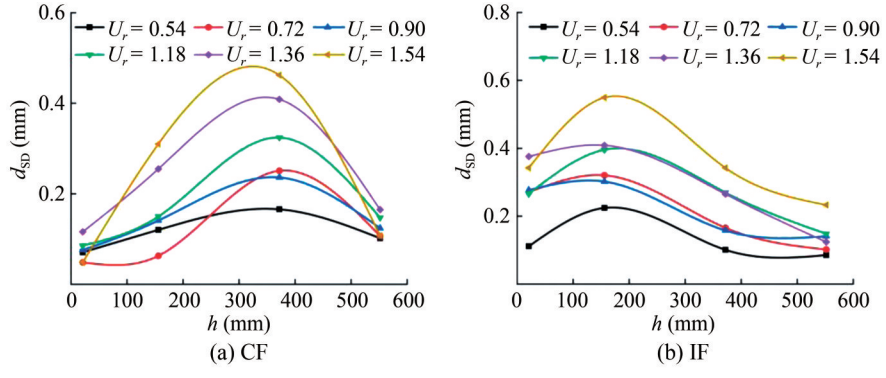

Figure 6 Spatial distribution of the displacement standard deviation in the CF and IL directions

3.3 Dimensionless dominant frequency of local position

Figures 7 and 8 display the variation of the dimensionless dominant frequency with the reduction velocity under shear flow. In addition, the dimensionless dominant frequency of different test positions was linearly fitted. The slope of the fitted line was the Strouhal number (St) in the test. The study of the dominant frequency in the CF and IL directions indicated that the dimensionless dominant frequency was less than the natural frequency of the underwater manipulator. The variation of the dimensionless dominant frequency was regular.

Figure 7 illustrates that the dimensionless dominant frequency in the CF direction increased with the reduction in velocity. The dimensionless dominant frequency in the CF direction was larger and closer to the natural frequency. At position 1, the dimensionless dominant frequency varied from 0.42 to 0.78, and the slope of the line after fitting was 0.33. The dimensionless dominant frequency of position 2 was further expanded to 0.54–0.80, and the St was 0.24. The dimensionless dominant frequency of position 3 was maintained between 0.40 and 0.76, and the St was 0.32. The dimensionless dominant frequency of position 4 was in the range of 0.39–0.69, and the St was 0.32. Different from the uniform flow, a significant influence on the Strouhal rule of flow around the circular cylinder under the shear flow field was observed (Huera-Huarte et al., 2014).

As shown in Figure 8, with the increase in velocity reduction under shear flow, the dimensionless dominant frequency in the IL direction increased, but the change in St was not evident. The reduction velocity was low in the test condition. Thus, the phenomenon that the response frequency in the IL direction was twice as much as that in the CF direction was not observed. At position 1, the variation range of the dimensionless dominant frequency was 0.42–0.63, and the Strouhal number was 0.18. The dimensionless dominant frequency at position 2 was 0.48–0.63, and the Strouhal number was 0.15. At position 3, the dimensionless dominant frequency was 0.35–0.64, and the Strouhal number was 0.31. The dimensionless dominant frequency at position 4 was 0.35 – 0.61, and the Strouhal number was 0.23. When the fluid flow through the underwater manipulator was placed at an angle, the vortex-induced vibration was affected by the complex section shape. This phenomenon was no longer consistent with the traditional law of Strouhal number (Chen et al., 2023).

Therefore, under the action of shear flow, the ratio between the CF and IL direction was close to 1. The Strouhal number also decreased evidently. The dimensionless dominant frequency in the CF and the IL directions varied from 0.39 to 0.80 and 0.35 to 0.64, respectively.

3.4 Displacement comparison between uniform and shear flow

Various postures of the underwater manipulator were observed during operation, corresponding to different flow fields. In addition to shear flow, uniform flow was a common flow field. When flow velocity U_r = 0.18, the displacement time history curve of the underwater manipulator under uniform and shear flow was compared to study the influence of flow fields on vortex-induced vibration.

Figure 9 presents the displacement time history curve of VIV at position 1 under different flow fields. Figure 10 depicts the displacement time history curve of the CF and IL direction at position 1 under different flow fields. In the uniform flow, the maximum displacement values in the CF and IL directions were 0.72 and 1.35 mm, respectively. At the same velocity under shear flow, the maximum displacement values in the CF and IL directions of the underwater manipulator were 1.47 and 2.29 mm, respectively. Under the influence of shear flow, the maximum displacement in the CF and IL directions increased by 104% and 70%,

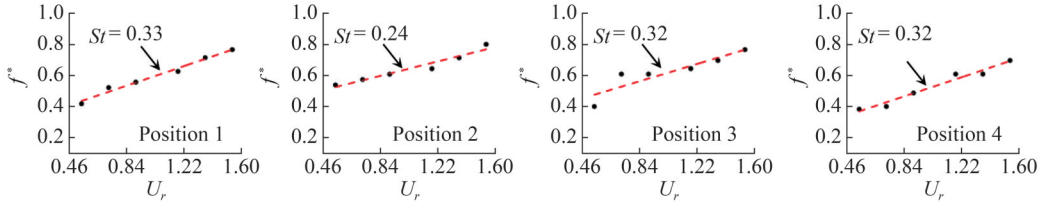

Figure 7 Dominant frequency of the CF vortex-induced vibration

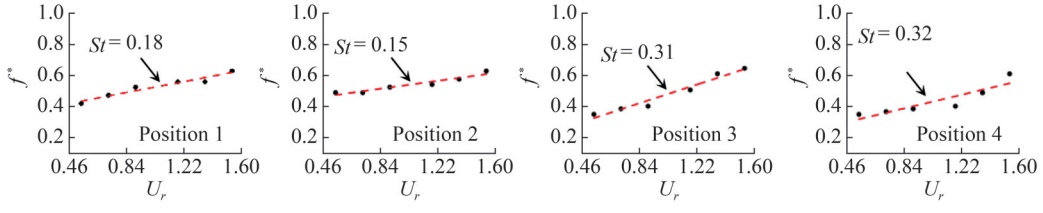

Figure 8 Dominant frequency of the IL vortex-induced vibration

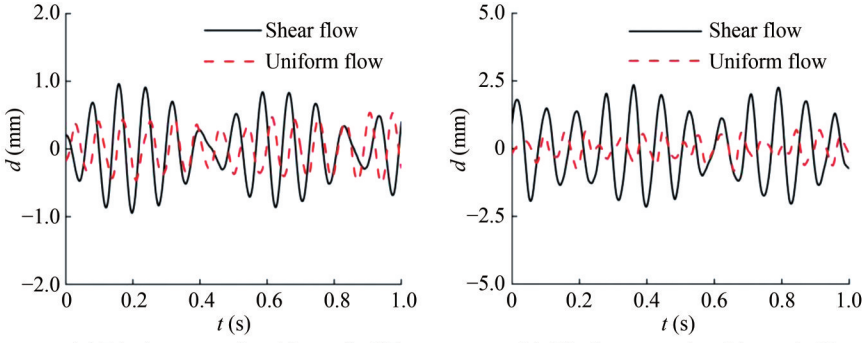

(a) Displacement time history in CF (b) Displacement time history in IL

Figure 9 Displacement time history curve of vortex-induced vibration at position 1 under different flow fields

respectively. The mean value of vibration displacement was further calculated. In the uniform flow, the mean displacement values in the CF and IL directions of the underwater manipulator were 0.24 and 0.29 mm, respectively. At the same velocity under shear flow, the mean displacement values in the CF and IL directions of the underwater manipulator were 0.50 and 1.05 mm, respectively. Compared with the uniform flow condition, the mean displacement increased by 110% and 20% in the CF and IL directions, respectively. The fluid excitation force varied with the change in the fluid. In uniform flow, the flow velocity around the underwater manipulator was consistent, resulting in a uniform drag distribution across the manipulator. Therefore, as shown in Figure 9, the displacement time history of the manipulator under uniform flow was stable. However, the flow velocity of the manipulator in the shear flow field changed along its arm, thereby increasing the drag inhomogeneity potential amplification of the drag (Song et al., 2016). At the same time, the interaction between the fluid and the underwater manipulator resulted in greater vibration responses and a "beating" phenomenon in the shear flow, attributed to the variable vortex shedding frequency along the arm (Lin et al., 2014).

The VIV response of the underwater manipulator under shear flow was greater than that in the uniform flow. In the shear flow, a certain effect on the increase in the maximum and mean displacements of vortex-induced vibration was observed. This phenomenon was more evident in the CF direction. When U_r = 0.18, the maximum and mean displacements of the shear flow to vortex-induced vibration increased by 104% and 110% at the highest, respectively. This condition adversely affects the stable operation of the underwater manipulator.

4 Conclusions

In this study, the vibration responses in the CF and IL directions of the underwater manipulator under shear flow fields at different positions were experimentally tested. The following conclusions were reached:

1) With the increase in reduction velocity, the dimensionless amplitude in the CF and IL directions of the underwater manipulator showed an upward trend. The vortex-induced vibration displacement reached the highest at 0.13D.

2) With the increase in test height, the displacement standard deviation of the underwater manipulator in both directions initially increased and then decreased, exhibiting a single mode. The vibration response of the underwater manipulator in the CF direction was mainly concentrated at positions 2 and 3, whereas the IL vibration response was concentrated at positions 1 and 2. When U_r = 1.54, the peak values in the CF and IL directions were 0.46 and 0.54 mm, respectively.

3) The VIV frequency of the underwater manipulator in the CF and IL directions increased with the reduction in velocity. The dimensionless frequencies in the two directions of the underwater manipulator were less than 1. The ratio of both directions was close to 1 at a lower velocity reduction. Moreover, the dimensionless dominant frequency in the CF and IL directions varied from 0.39–0.80 and 0.35–0.64, respectively.

4) Compared with uniform flow, the maximum and average values of VIV displacement increased under shear flow, especially in the CF direction. When U_r = 0.18, the increase in the maximum and average values of VIV displacement was up to 104% and 110%, respectively.

Finally, combined with the research conclusions, the VIV of the underwater manipulator in the shear flow field can improve the underwater kinematics model and provide preliminary basic research on the operation of the underwater manipulator in the marine environment. In the future, related research can be extended to the vibration response law of multi-posture underwater manipulators, improving the hydrodynamic model of this underwater manipulator. It provides a theoretical basis for the precise positioning and control of underwater manipulators.

Funding Supported by the National Natural Science Foundation of China (No. 51905211) and the "20 Regulations for New Universities" of Jinan (No. 202228116).

Competing interest The authors have no competing interests to declare that are relevant to the content of this article.

References

Allen DW, Henning DL (2001) Prototype vortex-induced vibration tests for production risers. Offshore Technology Conference, OTC-13114-MS. https://doi.org/10.4043/13114-ms

Aswathy MS, Sarkar S (2019) Effect of stochastic parametric noise on vortex induced vibrations. International Journal of Mechanical Sciences 153: 103-118. https://doi.org/10.1016/j.ijmecsci.2019.01.039

Bahmani MH, Akbari MH (2010) Effects of mass and damping ratios on VIV of a circular cylinder. Ocean Engineering 37(5-6): 511-519. https://doi.org/10.1016/j.oceaneng.2010.01.004

Capell NA, Carlson DW, Modarres-Sadeghi Y (2019) Vortex-induced vibration of a single degree-of-freedom flexibly-mounted horizontal cylinder near the free surface. Journal of Sound and Vibration 444: 161-175. https://doi.org/10.1016/j.jsv.2018.12.021

Carlucho I, Stephens DW, Barbalata C (2021) An adaptive data-driven controller for underwater manipulators with variable payload. Applied Ocean Research 113: 102726. https://doi.org/10.1016/j.apor.2021.102726

Chen W, Wang H, Chen C (2023) Experimental investigation of the vortex-induced vibration of a circular cylinder near a flat plate. Ocean Engineering 272: 113794. https://doi.org/10.1016/j.oceaneng.2023.113794

Chen WL, Zhang QQ, Li H, Hu H (2015) An experimental investigation on vortex induced vibration of a flexible inclined cable under a shear flow. Journal of Fluids and Structures 54: 297-311. https://doi.org/10.1016/j.fluidstructs.2014.11.007

Cheng Y, Duan D, Liu X, Yang X, Zhang H, Han Q (2022) Numerical study on hydrodynamic performance of underwater manipulator in the subcritical region. Ocean Engineering 262: 112214. https://doi.org/10.1016/j.oceaneng.2022.112214

de Wilde JJ, Huijsmans RHM (2004) Laboratory investigation of long riser VIV response. The Fourteenth International Offshore and Polar Engineering Conference, Toulon, Frunce, 511-516

Duan D, Cheng Y, Liu X, Yang X, Zhang H, Han Q (2023) Study on the effect of inflow direction on the hydrodynamic characteristics of underwater manipulators. Ocean Engineering 284: 115221. https://doi.org/10.1016/j.oceaneng.2023.115221

Fu X, Fu S, Ren H, Xie W, Xu Y, Zhang M, Liu Z, Meng S (2022) Experimental investigation of vortex-induced vibration of a flexible pipe in bidirectionally sheared flow. Journal of Fluids and Structures 114: 103722. https://doi.org/10.1016/j.jfluidstructs.2022.103722

Gao Y, Fu S, Xiong Y, Yang J, Wang M (2016) Experimental study on vortex induced vibration responses of a flexible cylinder in sheared current. Journal of Vibration and Shock 35(20): 142-148. https://doi.org/10.13465/j.cnki.jvs.2016.20.023

Gao Z, Efthymiou M, Cheng L, Zhou T, Minguez M, Zhao W (2020) Hydrodynamic damping of a circular cylinder at low KC: experiments and an associated model. Marine Structures 72: 102777. https://doi.org/10.1016/j.marstruc.2020.102777

Gopalkrishnan R (1993) Vortex-induced forces on oscillating bluff cylinders. Woods Hole Oceanographic Institution

Griffin OM, Vandiver JK (1984) Vortex-induced strumming vibrations of marine cables with attached masses. Journal of Energy Resources Technology 106(4): 458. https://doi.org/10.1115/1.3231106

Huera-Huarte FJ, Bangash ZA, González LM (2014) Towing tank experiments on the vortex-induced vibrations of low mass ratio long flexible cylinders. Journal of Fluids and Structures 48: 81-92. https://doi.org/10.1016/j.jfluidstructs.2014.02.006

Kang Z, Ni W, Sun L (2016) An experimental investigation of two-degrees-of-freedom VIV trajectories of a cylinder at different scales and natural frequency ratios. Ocean Engineering 126: 187-202. https://doi.org/10.1016/j.oceaneng.2016.08.020

Kolodziejczyk W (2016) Some considerations on an underwater robotic manipulator subjected to the environmental disturbances caused by water current. Acta Mechanica et Automatica 10(1): 43-49. https://doi.org/10.1515/ama-2016-0008

Kolodziejczyk W (2018) The method of determination of transient hydrodynamic coefficients for a single DOF underwater manipulator. Ocean Engineering 153: 122-131. https://doi.org/10.1016/j.oceaneng.2018.01.090

Kolodziejczyk W, Kolodziejczyk M, Kuzmierowski T, Qstazewski M (2023) Transient hydrodynamic coefficient for a single DOF underwater manipulator of square cross-section. Ocean Engineering 268: 113438. https://doi.org/10.1016/j.oceaneng.2022.113438

Kumar RP, Nallayarasu S (2022) VIV response of risers with large aspect ratio and low rigidity using a numerical scheme based on wake oscillator model. Applied Ocean Research 118: 103011. https://doi.org/10.1016/j.apor.2021.103011

Lin W, Chen Z, Yu J, Zheng X (2014) Analysis of vortex-induced vibration and heat transfer of an elastic cylinder at low Reynolds numbers. Applied Mechanics and Materials 602: 458-464. https://doi.org/10.4028/AMM.602-605.458

Liu Y, Li P, Wang Y, Guo H, Zhang X (2020) Experimental investigation on the vortex-induced vibration of the vertical riser fitted with the water jetting active vibration suppression device. International Journal of Mechanical Sciences 177: 105600. https://doi.org/10.1016/j.ijmecsci.2020.105600

Liu Y, Liu J, Gao FP (2023) Strouhal number for boundary shear flow past a circular cylinder in the subcritical flow regime. Ocean Engineering 269: 113574. https://doi.org/10.1016/j.oceaneng.2022.113574

Mao L, Liu Q, Zhou S, Jiang W, Liu Z, Peng T (2015) Vortex-induced vibration mechanism of drilling riser under shear flow. Petroleum Exploration and Development 42(1): 112-118. https://doi.org/10.1016/s1876-3804(15)60013-1

Mao L, Yan J, Zeng S, Cai M (2023) Vortex-induced vibration characteristics of mining riser under the coupling effect of external ocean current and internal multiphase flow. Applied Ocean Research 140: 103747. http://doi.org/10.1016/j.apor.2023.103747

McLain TW, Rock SM (1998) Development and experimental validation of an underwater manipulator hydrodynamic model. The International Journal of Robotics Research 17(7): 748-759. https://doi.org/10.1177/027836499801700705

Mercier JA (1973) Large amplitude oscillations of a circular cylinder in a low-speed stream. PhD thesis, Stevens Institute of Technology, Hoboken, 21-30

Sarpkaya T (1977) Transverse oscillations of a circular cylinder in uniform flow, Part 1. PhD thesis, Naval Postgraduate School, Monterey, 1-9

Seyed-Aghazadeh B, Anderson N, Dulac S (2021) Flow-induced vibration of high-mass ratio isolated and tandem flexible cylinders with fixed boundary conditions. Journal of Fluids and Structures 103: 103276. https://doi.org/10.1016/j.jfluidstructs.2021.103276

Song L, Fu S, Dai S, Zhang M, Chen Y (2016) Distribution of drag force coefficient along a flexible riser undergoing VIV in sheared flow. Ocean Engineering 126: 1-11. https://doi.org/10.1016/j.oceaneng.2016.08.022

Sun H, Li H, Yang N, Hou G, Bernitsas M (2023) Experimental and numerical study of the shielding effect of two tandem rough cylinders in flow-induce oscillation. Marine Structures 89: 103374. https://doi.org/10.1016/j.marstruc.2023.103374

Tognarelli MA, Slocum ST, Frank WR, Campbell RB (2004) VIV response of a long flexible cylinder in uniform and linearly sheared currents. Offshore Technology Conference, OTC-16338-MS. https://doi.org/10.4043/16338-ms

Wang Y, Zhang Z, Bingham HB, Xu F (2022) Numerical simulation of vortex-induced vibrations of inclined flexible risers subjected to uniform current. Applied Ocean Research 129: 103408. http://doi.org/10.1016/j.apor.2022.103408

Wu Q, Yang J, Guo X, Liu L, Lu W, Lu H (2022) Experimental study on dynamic responses of a deep-sea mining system. Ocean Engineering 248: 110675. https://doi.org/10.1016/j.oceaneng.2022.110675

Xue H, Yuan Y, Tang W (2019) Numerical investigation on vortex-induced vibration response characteristics for flexible risers under sheared-oscillatory flows. International Journal of Naval Architecture and Ocean Engineering 11(2): 923-938. https://doi.org/10.1016/j.ijnaoe.2019.05.001

Zhang C, Kang Z, Stoesser T, Xie Z, Massie L (2020) Experimental investigation on the VIV of a slender body under the combination of uniform flow and top-end surge. Ocean Engineering 216: 108094. https://doi.org/10.1016/j.oceaneng.2020.108094

Zhu H, Zhao H, Srinil N (2021) Experimental investigation on vortex-induced vibration and solid-structure impact of a near-bottom horizontal flexible pipeline in oblique shear flow. Journal of Fluids and Structures 106: 103356. https://doi. org/10.1016/j.jfluidstructs.2021.103356

Zhu W, Zhang Y, Zhang H, Di Q (2022) Lock-in in the vortex-induced vibrations of a long tensioned riser in internal fluid flow and external uniform and shear flows: A prediction based on models. Journal of Sound and Vibration 530: 116970. https://doi.org/10.1016/j.jsv.2022.116970